Interconversions of nitrogen-containing species on Pt(100) and Pt(111) electrodes in acidic solutions containing nitrate

Katsounaros, I.; Costa Figueiredo, M.C.; Chen, X.; Calle Vallejo, F.; Koper, M.T.M.

Electrochimica Acta 271 (2018) 77–83

Contents lists available at ScienceDirect

Electrochimica Acta

journal homepage: www.elsevier.com/locate/electacta

Interconversions of nitrogen-containing species on Pt(100) and Pt(111) electrodes in acidic solutions containing nitrate

Ioannis Katsounaros [a, *, 1], Marta C. Figueiredo [a], Xiaoting Chen [a], Federico Calle-Vallejo [b], Marc T.M. Koper [a, **]

[a] Leiden University, Leiden Institute of Chemistry, Einsteinweg 55, 2333CC Leiden, The Netherlands
[b] Departament de Ciència de Materials i Química Física & Institut de Química Teòrica i Computacional (IQTCUB), Universitat de Barcelona, Martí i Franqués 1, 08028 Barcelona, Spain

ARTICLE INFO

Article history:
Received 13 February 2018
Received in revised form
15 March 2018
Accepted 20 March 2018
Available online 22 March 2018

Keywords:
Nitrate reduction
Platinum
Single-crystal electrochemistry
Nitrogen cycle

ABSTRACT

This work deals with the interconversions of various nitrogen-containing compounds on Pt(111) and Pt(100) electrodes in contact with acidic solutions of nitrate. Via its reduction, nitrate acts merely as the source of adsorbed nitrogen-containing intermediates, which then undergo complex oxidative or reductive transformations depending on the electrode potential. Nitrate reduction to ammonium is structure sensitive on Pt(111) and Pt(100) because it is mediated by *NO, the adsorption and reactivity of which is also structure sensitive. Accordingly, previous knowledge from *NO electrochemistry is useful to streamline nitrate reduction and elaborate a comprehensive picture of nitrogen-cycle electrocatalysis. Our overall conclusion for nitrate reduction is that the complete conversion to ammonium under prolonged electrolysis is possible only if the reduction of nitrate to nitric oxide, and the reduction of nitric oxide to ammonium are feasible at the applied potential. Among the two surfaces studied here, this condition is fulfilled by Pt(111) in a narrow potential region.

1. Introduction

Electrochemical reactions involving nitrogen-containing compounds have been traditionally attractive to understand fundamentals of electrochemical surface science and electrode kinetics [1–3]. Such reactions include (but are not limited to) nitrate reduction, nitric oxide reduction and oxidation [4,5], nitrous oxide reduction [6,7] or ammonia oxidation [8,9]. Apart from their fundamental importance, some of the above reactions may additionally have potential applications in the fields of wastewater treatment [10–12], electrochemical sensors [13], electrochemical synthesis [14], and energy conversion [15]. Overall, the reactions of nitrogen-containing compounds are complicated, as they typically involve several bond-breaking or bong-forming events and thus several intermediates and final products are formed. These processes are in fact interconnected within the biogeochemical nitrogen cycle and often share the same intermediates [16].

The reduction of nitrate exemplifies the complexity of the electrocatalysis of the nitrogen cycle. This reaction has been investigated on several monometallic [17–23], bimetallic [23–26] or modified [3,27–30] electrodes in which various final products such as nitrite, NO, N_2O, N_2, NH_2OH or NH_3 can be formed. Platinum single-crystal electrodes have also been utilized to understand structural effects on the reactivity and product distribution [2,31–34].

Herein, we study the voltammetric and spectroscopic behaviour of Pt(111) and Pt(100) electrodes in acidic solutions containing nitrate. Our focus is placed on the formation of adsorbed intermediates and desorbed products as a function of the electrode potential. We use classical electrochemical techniques, vibrational spectroscopy as well as density functional theory (DFT) calculations. We show that adsorbed nitrogen-containing species that originate from nitrate reduction undergo complex, potential-driven transformations which are structure sensitive. The electrochemical behaviour is eventually controlled by the reactivity of these

* Corresponding author.Present address: Forschungszentrum Jülich GmbH, Helmholtz Institute Erlangen-Nürnberg for Renewable Energy (IEK-11), Egerlandstraße 3, 91058 Erlangen, Germany.
** Corresponding author.
E-mail addresses: i.katsounaros@fz-juelich.de (I. Katsounaros), m.koper@lic.leidenuniv.nl (M.T.M. Koper).
[1] Present address: Forschungszentrum Jülich GmbH, Helmholtz Institute Erlangen-Nürnberg for Renewable Energy (IEK-11), Egerlandstraße 3, 91058 Erlangen, Germany.

https://doi.org/10.1016/j.electacta.2018.03.126

adsorbates and nitrate in solution merely provides the surface with such adsorbates. Therefore it is anticipated that the findings of this study can be extended to other electrocatalytic reactions relevant to the nitrogen cycle which form the same intermediate species.

2. Experimental methods

The electrochemical measurements were performed in a glass electrochemical cell. The working electrodes were Pt beads (Prof. Juan Feliù, University of Alicante) in the hanging meniscus configuration. Prior to each measurement, the crystal was flame-annealed and cooled to room temperature in an Ar:H_2 (3:1) environment, in accordance to a well-established methodology [35,36]. The clean, well-ordered single-crystal electrode was immersed in the solution at +0.07 V_{RHE}, unless otherwise stated. The voltammograms always represent the first cycle after annealing, starting from +0.07 V_{RHE} to the positive direction, unless otherwise stated. The counter electrode was a Pt wire, also flame-annealed before the measurement, and the reference was a reversible hydrogen electrode (RHE).

The Fourier transform infrared spectroscopy experiments were performed with a Bruker Vertex 80v vacuum spectrometer in the external reflection mode, using an MCT detector and *p*-polarization, in the thin-layer configuration using a spectroelectrochemical cell similar to the one described previously [37]. The working electrode for these measurements was a platinum single-crystal disk from Mateck GmbH, prepared as described for the Pt beads in the previous paragraph. Each spectrum represents the average of 100 interferograms collected with a resolution of 8 cm^{-1}. The spectra were intentionally recorded under potentiostatic conditions to allow a high signal-to-noise ratio while being at a steady state. The spectra are shown as $(R-R_0)/R_0$, where R and R_0 are the reflectance at the sample and reference potential, respectively. Therefore, positive bands correspond to species in excess at the sample potential with respect to the reference potential and negative bands to species in deficiency at the sample potential with respect to the reference potential.

"Online" ion chromatography was performed in accordance to the methodology described by Yang et al. [38]. The methodology for the formation of NO adlayers and subsequent reductive stripping has been described previously [5].

An Autolab PGSTAT302 N potentiostat was used for the potential control and the current measurement. Compensation for the electrolyte resistance was done with positive feedback. The measurements were performed at room temperature in an electrolyte saturated with Argon. The current was normalized to the geometric area of the working electrode.

The electrolyte was always freshly prepared using ultrapure water (Merck Millipore®, 18.2 MΩ, TOC < 3 ppb) and concentrated perchloric acid (Merck Suprapur®, 70%). The gases used were 6 N quality (Airgas Inc.). All glassware was cleaned in an acidic solution of potassium permanganate overnight, followed by rinsing with an acidic solution of hydrogen peroxide and repetitive rinsing and boiling with ultrapure water.

Computationally, the free energy was approximated as: $G \approx E_{DFT} + ZPE - TS + E_{solvation}$. The DFT total energies (E_{DFT}), zero-point energies (*ZPE*) and entropy terms (*TS*) of *N, *NH, *NHO, *NOH, *NHOH and *NO at Pt(100) were taken from a previous study [5]. The solvation corrections ($E_{solvation}$) were taken from the work of Greeley and co-workers [39] and the energy of protons and electrons was assessed by means of the computational hydrogen electrode [40], which allows reporting the adsorption energies in Fig. 6 at a potential of 0.75 V. Note that the calculated adsorption energies in Fig. 6 use a different reference with respect to previous studies: here we consider as a reference the reactants of the elementary step under consideration.

3. Results and discussion

3.1. Nitrate reduction on Pt(111)

The voltammetries in 0.1 M $HClO_4$ solutions with and without nitrate on Pt(111) are shown in Fig. 1 (solid and dotted curve, respectively). The "blank" (nitrate-free) voltammogram exhibits the typical features of a well-ordered Pt(111) electrode in this solution [36]. When scanning from +0.07 V_{RHE} in the positive direction (solid black curve), nitrate reduction starts above +0.25 V_{RHE} (R_1^{111}), following desorption of hydrogen, which inhibits the reaction at less positive potentials. The reductive current is maximized at +0.35 V_{RHE} and then decreases, probably because intermediates of nitrate reduction remain adsorbed and are not further reduced. The complete suppression of the *OH-related "butterfly" features at ca. +0.8 V_{RHE} [36] indicates that such blocking species are not only stable between ca. +0.45 to +0.85 V_{RHE} but also detrimental for *OH adsorption.

In the reverse scan (solid gray curve in Fig. 1), significant processes are observed again only below +0.45 V_{RHE} with two reductive waves centered at ca. +0.32 V_{RHE} (R_2^{111}) and ca. +0.1 V_{RHE} (R_3^{111}). The voltammetric profile resembles the reductive *NO stripping from Pt(111) (red dashed curve for a full *NO layer, shown for comparison) [5]. Thus, we attribute R_2^{111} and R_3^{111} to the reduction of *NO formed from nitrate reduction during the positive-going scan. Besides, *NO is the species responsible for the suppression of the "butterfly" features. The two waves are related to the reduction of *NO adsorbed at on-top (R_2^{111}) and fcc-hollow (R_3^{111}) sites [41]. From the comparison of the charge densities in nitrate-containing solution and in the Pt(111)-NO layer for each peak (i.e. compare solid gray and dashed red curve for both peaks), we conclude that the *NO formed from nitrate reduction is nearly at saturation on the fcc-hollow sites while the coverage on the top sites is significantly lower. The preference of the formed *NO for the fcc-hollow sites is related to the fact that this is the most stable

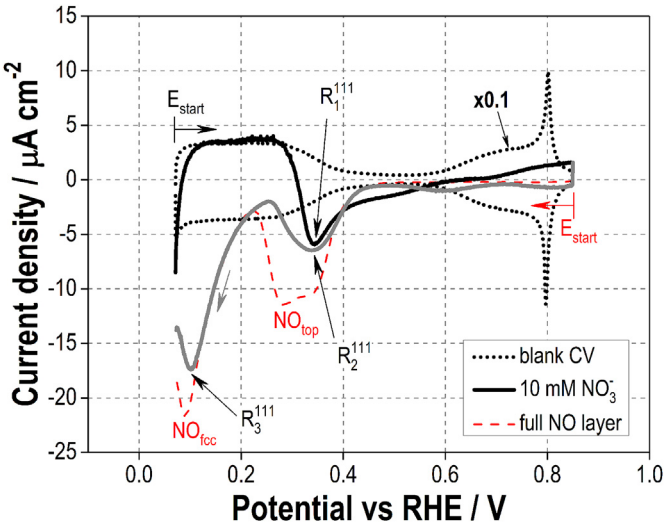

Fig. 1. Cyclic voltammetry (5 mV s^{-1}) on Pt(111) in 0.1 M $HClO_4$ + 0.01 M $NaNO_3$ (solid curve). Black and gray colors are used to distinguish between the positive and negative directions of the sweep, respectively. The "blank" voltammogram in nitrate-free 0.1 M $HClO_4$ is shown for comparison (dotted curve, 50 mV s^{-1}, the measured current was multiplied by 0.1). The red dashed curve corresponds to the linear sweep voltammogram (5 mV s^{-1}) of a saturated NO adlayer, starting from +0.85 V_{RHE}. (For interpretation of the references to color in this figure legend, the reader is referred to the Web version of this article.)

adsorption site for *NO on Pt(111), followed by atop *NO [5]. Therefore, the surface blockage observed during a potential cycle occurs because nitrate reduction forms the blocking species (*NO on the fcc-hollow site) at a potential where *NO is stable and requires a more negative potential for its reduction.

We recorded the FTIR spectra at different potentials in the nitrate-containing solution (see Fig. S1 in the Supporting Information, SI) but did not observe any band for NO in the entire potential region. This is reasonable because the N-O stretching from *NO on the fcc-hollow site is known to have a very low intensity, while atop *NO, which can be observed with infrared spectroscopy, has a low coverage here from nitrate reduction [5]. Remarkably, a positive band was observed at ca. 2343 cm^{-1} for a potential step from +0.4 to +0.85 V_{RHE} (Fig. S1). We assign this band to hyponitrous acid (HON=NOH), based on the transmission spectrum recorded in a 0.1 M $HClO_4$ + 0.01 M *trans*-$Na_2N_2O_2$ solution (Fig. S2). The conjugate base of hyponitrous acid, the hyponitrite ion ($N_2O_2^{2-}$) has previously been identified as an intermediate of nitrate reduction on tin, in alkaline solution [22]. The detection of $H_2N_2O_2$ here is a strong evidence of nitrate reduction via *NOH, i.e. the precursor of hyponitrous acid [42].

3.2. Nitrate reduction on Pt(100)

Similar to Pt(111), the reduction of nitrate on Pt(100) commences only after hydrogen desorption at ca. +0.3 V_{RHE}, as concluded by comparison between the voltammograms in nitrate-free (dotted curve) and nitrate-containing solutions (solid curve) in Fig. 2. The reduction reaction is associated with a very sharp peak (R_1^{100}) at ca. +0.34 V_{RHE} in the positive-going scan. The introduction of only a small density of (110) steps on Pt(100) is detrimental for the intensity of the R_1^{100} peak, suggesting that the reduction of nitrate in the region of the sharp peak takes place predominantly on (100) terraces (see Fig. S3 for Pt(10 1 0)). In addition, the R_1^{100} peak current density scales linearly with the scan rate (in the range 1–50 mV s^{-1}) which implies that the current is controlled by a surface process (see Fig. S4a).

The FTIR spectra in H_2O and D_2O (Fig. 3a and b, respectively) for a potential step from $E_{reference}$ = +0.2 V to E_{sample} = +0.4 V (spectra in red) show only a strong negative band at ca. 1360 cm^{-1} attributed to the depletion of nitrate during this potential step. We did not observe any NH_4^+ characteristic band at ca. 1460 cm^{-1} in H_2O, between +0.2 and +0.4 V_{RHE}, while "online" chromatography did not provide any evidence that ammonium forms during the R_1^{100} peak, either. In addition, if the potential scan is limited between +0.3 and +0.4 V_{RHE}, the otherwise sharp R_1^{100} disappears already from the second scan (see Fig. S5). The above observations indicate that ammonium is not a major product of the reduction of nitrate in the R_1^{100} peak, but instead the reduction is accompanied with the adsorption of inactive nitrogen-containing intermediates that suppress the reaction.

In the potential region from +0.4 to +0.65 V_{RHE} (still in the positive-going scan) the reaction takes place with a low rate, as seen in the voltammogram in Fig. 2 where a small reduction current is recorded. This corroborates with the spectra at E_{sample} = +0.65 V with $E_{reference}$ = +0.4 V in H_2O and D_2O (Fig. 3, spectra in green) which show the formation of products of nitrate reduction. In particular, the spectrum in Fig. 3a (i.e. in H_2O) shows a positive band at 2343 cm^{-1} assigned to $H_2N_2O_2$, which again indicates that *NOH forms as the precursor of hyponitrous acid. In addition, a positive band is observed at 1570 cm^{-1} in Fig. 3b (i.e. in D_2O) and is assigned to low-coverage *NO adsorbed on bridge sites [5]. The origin of *NO is probably from the HNO_2 produced by nitrate reduction, as HNO_2 is known to disproportionate in acidic solution.

While on Pt(111) *NO is reduced at more negative potentials

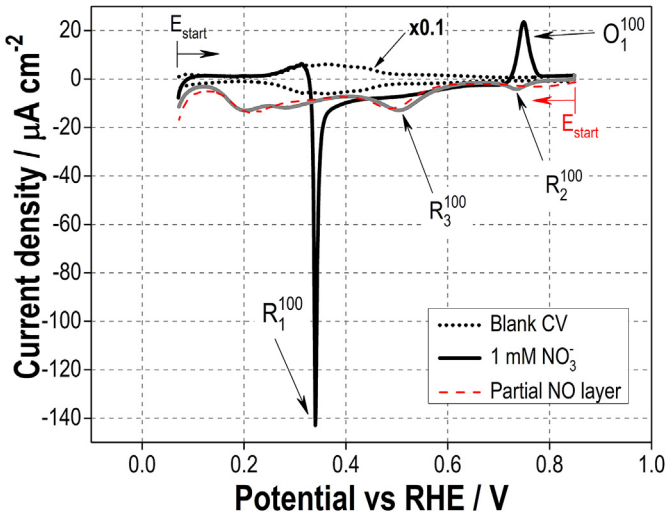

Fig. 2. Cyclic voltammetry (5 mV s^{-1}) on Pt(100) in 0.1 M $HClO_4$ + 0.001 M $NaNO_3$ (solid curve). Black and gray are used to distinguish between the positive and negative directions of the sweep, respectively. The red dashed curve corresponds to the linear sweep voltammogram (5 mV s^{-1}) of a non-saturated NO adlayer, starting from +0.85 V_{RHE}. The "blank" voltammogram in nitrate-free 0.1 M $HClO_4$ is shown for comparison (dotted curve, 50 mV s^{-1}, the measured current was multiplied by 0.1). (For interpretation of the references to color in this figure legend, the reader is referred to the Web version of this article.)

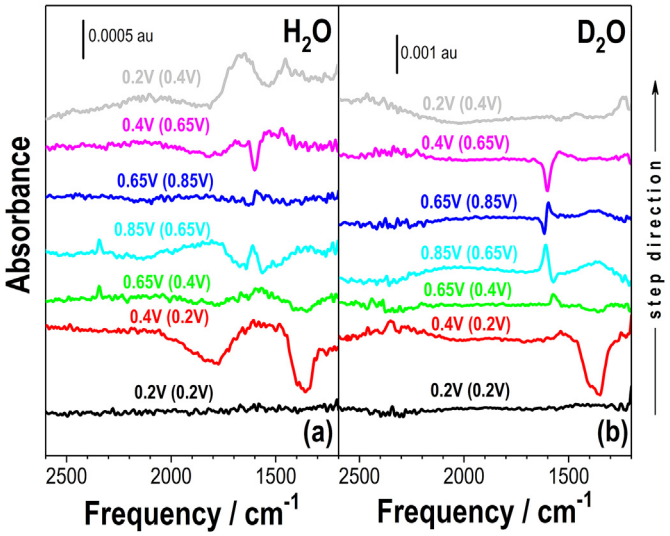

Fig. 3. Infrared spectra recorded for Pt(100) in (a) H_2O and (b) D_2O, in 0.1 M $HClO_4$ + 0.01 M $NaNO_3$. The sample potential is indicated in the legends and the reference potential in brackets. The arrow at the right side of the figure indicates the direction of the steps.

than nitrate, on Pt(100) low-coverage *NO can be reduced in the potential region of nitrate reduction, via *NHO, *N and *NH_x as shown previously [5]. Since we detect *NO in this potential region with the infrared measurements, it is likely that such *NO partially undergoes reduction to any of the above species.

A further increase of the potential in the voltammetry leads to an oxidative peak centered at +0.75 V_{RHE} (O_1^{100}) (Fig. 2). The peak current is linearly dependent on the scan rate which points to a surface-confined process (Fig. S4b). In the infrared spectra, an asymmetric bipolar band is observed at +0.85 V_{RHE} in D_2O (with reference at +0.65 V, spectrum in cyan in Fig. 3b), with a small negative component at ca. 1570 cm^{-1} and a large positive

component at ca. 1610 cm^{-1}. The shift of the NO band from 1570 to 1610 cm^{-1} as well as the asymmetric character of the bipolar band are clear indications that *NO coverage increased substantially from +0.65 V to +0.85 V [5]. The increase in *NO coverage during the O_1^{100} peak is significant enough to observe a positive band at 1610 cm^{-1} even in H_2O (Fig. 3a, spectrum in cyan) where *NO detection is typically more difficult because of interference from water bands [5].

The reaction that leads to *NO formation during the O_1^{100} peak involves the oxidation of a nitrogen-containing adsorbate, hereafter denoted $N_xH_yO_z$, which forms previously from nitrate reduction (i.e. at any potential before the O_1^{100} peak). The oxidation state of nitrogen in $N_xH_yO_z$ is lower than +2, because *NO is a product of the oxidation of $N_xH_yO_z$. When nitrate concentration increases in solution, it is likely that its reduction results in higher *NO coverage. From a previous study, we showed that *NO is more stable towards reduction to *NHO on Pt(100) when its coverage is higher [5]. Here, we find that the O_1^{100} peak diminishes by increasing the nitrate concentration (see Fig. 4). A reasonable interpretation of this observation is that the more compact and more stable *NO adlayer from the reduction of nitrate at higher concentrations is detrimental for the formation of $N_xH_yO_z$, e.g. because *NO reduction is inhibited when *NO coverage increases. Considering that the product of *NO reduction at low coverages is *NHO [5], a likely candidate for $N_xH_yO_z$ is *NHO.

Apart from *NO, $H_2N_2O_2$ is again observed with a band at 2343 cm^{-1} in the potential step from +0.65 V to +0.85 V, which suggests that hyponitrous acid is still formed above +0.65 V_{RHE} (Fig. 3a, spectrum in cyan).

During the negative-going scan (solid gray curve in Fig. 2), a small reductive peak is observed at +0.735 V_{RHE} (R_2^{100}). The infrared spectroscopy at +0.65 V_{RHE} (reference at +0.85 V_{RHE}) shows a bipolar band for *NO, mainly due to the Stark effect (Fig. 3b, spectrum in blue). When the crystal was immersed in nitrate solution at +0.85 V_{RHE} immediately after annealing in a separate experiment, i.e. without prior reduction of nitrate at lower potentials and subsequent adsorption of any reaction products, we observed the following: (i) the R_2^{100} peak was much more pronounced compared to the experiment in Fig. 2a (Fig. 5); (ii) NO formation was observed during the step from +0.85 V to +0.65 V by infrared spectroscopy (inset a in Fig. 5); (iii) the R_2^{100} peak current is linearly dependent on the scan rate (inset b in Fig. 5); and (iv) the peak position depends on the logarithm of the concentration of nitrate in solution (inset c in Fig. 5). Based on all of the above, we assign the R_2^{100} peak to the reduction of nitrate to *NO, in agreement with a previous hypothesis [34]. This proposition is consistent with the standard potential of the $HNO_3(l)/NO(g)$ couple (+0.957 V_{RHE}) which must be even more positive for the $HNO_3(l)$/*NO couple considering the strongly exothermic adsorption of NO on Pt(100).

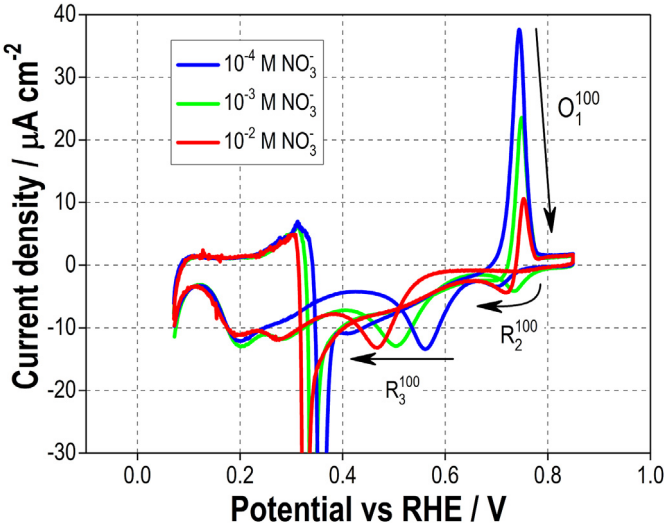

Fig. 4. Cyclic voltammetry (5 mV s^{-1}) on Pt(100) in 0.1 M $HClO_4$ with different concentrations of nitrate. The arrows are used as a guide to the eye for the dependence of the O_1, R_2 and R_3 peaks as the concentration of nitrate increases.

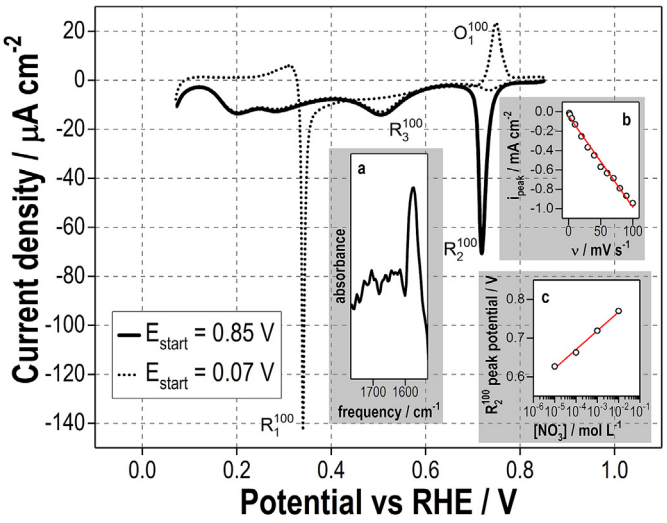

Fig. 5. Cyclic voltammetry (5 mV s^{-1}) on Pt(100) in 0.1 M $HClO_4$ + 0.001 M $NaNO_3$, starting from +0.07 V_{RHE} (dotted curve) or from +0.85 V_{RHE} (solid curve). Inset (a): Infrared spectrum at +0.65 V_{RHE} with the reference potential at +0.85 V_{RHE} for a solution of 0.01 M $NaNO_3$, when the contact of the annealed electrode with the solution was done at +0.85 V_{RHE}. Inset (b): Scan rate dependence of the peak current for nitrate reduction when the measurement started from +0.85 V_{RHE}. Inset (c): Concentration dependence of the peak potential for nitrate reduction when the measurement started from +0.85 V_{RHE}.

The reduction of nitrate to *NO during the R_2^{100} peak takes place on platinum sites that were not available before the O_1^{100} peak. Otherwise, the reaction would have already taken place at the more favoring lower potentials during the positive-going scan. The increased site availability after the O_1^{100} peak reveals that the *$N_xH_yO_z$ species occupies more platinum atoms than the produced *NO, so the *$N_xH_yO_z$ oxidation to *NO results in unoccupied Pt sites which are free for nitrate reduction to *NO in the negative-going scan. This claim is also supported by the fact that the R_2^{100} peak diminishes by increasing the HNO_3 concentration (see Fig. 4), as higher nitrate concentrations lead to higher *NO coverage already from nitrate reduction in the positive-going scan, as mentioned already above, at the expense of other nitrogen-containing compounds.

Previous electronic-structure calculations showed that at low and relatively high coverage, *NO is a bridged adsorbate on Pt(100), so that each *NO occupies two Pt atoms [5]. In an attempt to determine the exact composition and structure of *$N_xH_yO_z$, we observe that the only nitrogen-containing adsorbates with nitrogen at an oxidation state lower than +2 and with higher occupancy than two surface Pt atoms are *NHO, *N and *NH. Note in passing that all of these three species adsorb on 4-fold hollow sites on Pt(100).

Fig. 6 contains four possible scenarios for *NO production at +0.75 V_{RHE}, a representative potential of the O_1^{100} peak in Fig. 2.

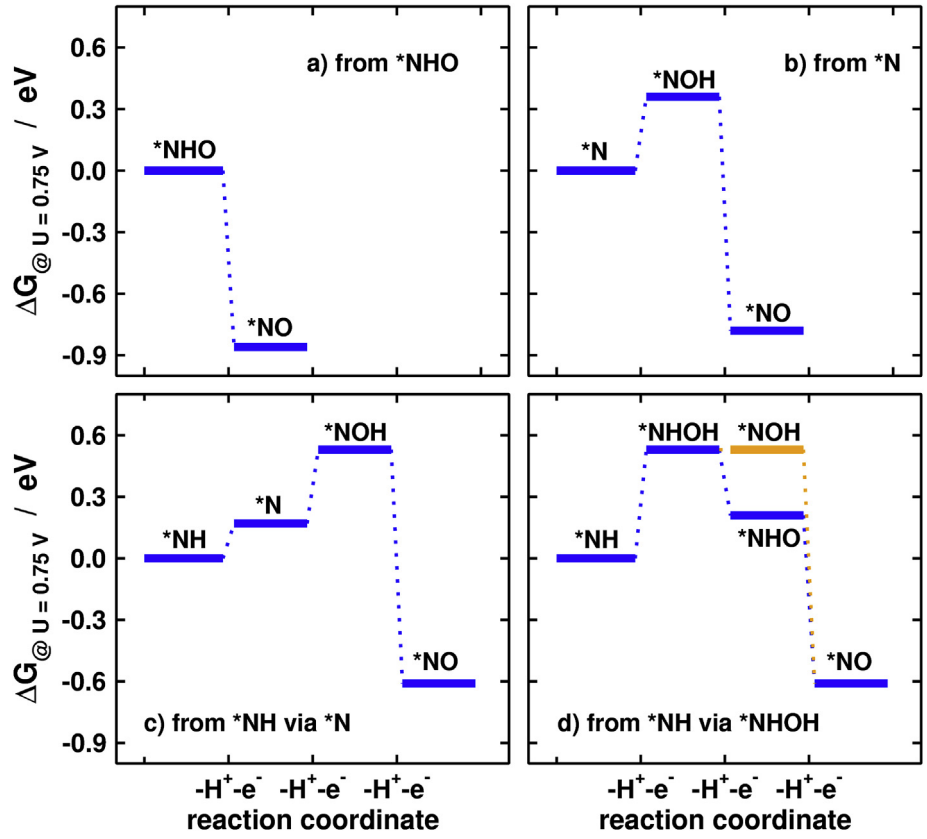

Fig. 6. Plausible pathways for *NO generation from *$N_xH_zO_y$-like adsorbates at +0.75 V_{RHE}. *NO is produced from a) *NHO, b) *N, c) *NH via *N, and d) *NH via *NHOH. In each panel, the initial adsorbate is used as a reference for the adsorption energies. A proton-electron pair is removed in each step.

Assuming that *NHO, *N and *NH are present at the surface at +0.75 V_{RHE} and that only downhill elementary steps are thermodynamically feasible at such potential, we evaluate the most favorable way of oxidizing them to *NO by means of electrochemical steps (see the details of the calculations in the Experimental methods section). According to Fig. 6, the oxidation of *NHO to *NO is entirely exothermic at +0.75 V_{RHE}, a representative potential of the O_1^{100} peak in Fig. 2. Conversely, the oxidation of either *N or *NH to *NO involves at least one endothermic step.

Therefore, we propose that the *$N_xH_zO_y$ adsorbate oxidized to *NO at the O_1^{100} peak is *NHO, most likely formed via *NO hydrogenation below ca. +0.6 V_{RHE}. This proposition is in agreement with the interpretation made above for the concentration dependence of the O_1^{100} peak. Moreover, the calculations do not exclude the possibility that *NOH be oxidized to *NO as well: in Fig. 6b–d the formation of *NOH from *N or *NH is endothermic, but its dehydrogenation to produce *NO is highly exothermic. However, *NO and *NOH adsorb both at bridge sites on Pt(100), which would not explain the observed increase in site availability.

In the potential region from +0.65 to +0.4 V_{RHE} in the negative-going scan a reduction wave (R_3^{100}) is observed in Fig. 2, and the infrared spectra in either H_2O or D_2O for the same potential region show unambiguously that the peak R_3^{100} is associated to the reduction of *NO (see negative band in Fig. 3a and b, spectrum in pink). The potential at which *NO is reduced here is more positive by ca. 250 mV than the potential in which a full *NO adlayer is reduced [43]. This is because the onset potential for *NO reduction at low coverage is more positive than for a saturated *NO adlayer, as also mentioned above [5]. For instance, the red dashed curve in Fig. 2 shows the response for the reduction of a partial Pt(100)-*NO layer in a clean (nitrate-free) solution. The increase in the concentration of nitrate leads to a shift in the position of R_3^{100} toward more negative potentials (see Fig. 4), which is an indication of higher *NO coverage by increasing nitrate concentration. The reduction of *NO at the R_3^{100} peak yields mainly a nitrogen-containing adsorbate: this is evident by the infrared spectra that show *NO depletion for the step from $E_{reference}$ = +0.65 V to E_{sample} = +0.4 V, though without a significant positive band for NH_4^+ (Fig. 3a, spectrum in pink).

Based on our previous conclusion that low-coverage *NO is reduced via *NHO [5], we hypothesize that the *NO formed is subsequently reduced to *NHO at the R_3^{100} peak. To prove this hypothesis, in separate experiments we restricted the low-potential limit (LPL) within the R_3^{100} region. Indeed, we found that the processes in the O_1^{100} and R_3^{100} peak are strongly connected: by using a more positive LPL (e.g. blue curve in Fig. 7) the charge for the O_1^{100} peak decreases. Therefore, we conclude that in the R_3^{100} peak *NO is reduced to *NHO, which is oxidized back to *NO in the O_1^{100} if the scan is reversed as in the measurements in Fig. 7.

Returning to Fig. 2, the surface is free from nitrogen-containing adsorbates in the negative-going scan, only at potentials below +0.4 V_{RHE}. A reductive process takes place at potentials around +0.2 V_{RHE}, and the infrared spectra show the formation of dissolved ammonium (see positive band at 1460 cm^{-1} in H_2O for the step from +0.4 V to +0.2 V, Fig. 3a, spectrum in gray).

3.3. Proposed mechanism

We propose here a scheme (Scheme 1) summarizing the structure-sensitive transformations of nitrogen-containing species

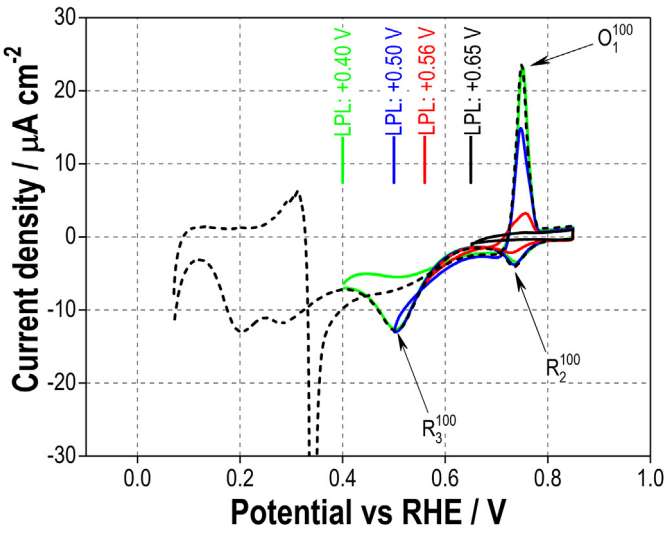

Fig. 7. Cyclic voltammograms with the same conditions as in Fig. 2, but restricting the low potential limit (LPL) within the region of *NO reduction to *NHO. The voltammogram with the LPL at +0.07 V_{RHE} is shown for comparison (dashed curve).

generated on single-crystal Pt(100) and Pt(111) from acidic nitrate solutions as described in the previous sections.

On both Pt(111) and Pt(100) the reaction starts from the deoxygenation (hydrogenation) of HNO_3 to HNO_2 once hydrogen desorption takes place, i.e. above ca. +0.25 to +0.3 V depending on the surface facet. In acidic solutions, HNO_2 disproportionates to HNO_3 and NO and the former is exothermically adsorbed on the Pt surfaces. The detection of hyponitrous acid in infrared spectroscopy on both facets indicates that in parallel with HNO_2 disproportionation, further deoxygenation of HNO_2 to *NOH and dimerization to $H_2N_2O_2$ takes place.

The reaction steps described so far are identical for Pt(111) and Pt(100), but the pathways diverge once adsorbed *NO is formed as a result of the structure-sensitive reduction of *NO [5]. On Pt(111), *NO adsorbed on top sites can be reduced to *NOH only below +0.4 V, while *NO adsorbed on the fcc-hollow sites is reduced at even less positive potentials (below +0.25 V).

In contrast, on Pt(100) *NO is reduced to *NHO at potentials below +0.60 V as long as the *NO layer is not saturated. *NHO is reduced to NH_4^+ at a less positive potential (below ca. +0.4 V) and oxidized to *NO at ca. +0.75 V. Therefore, once *NHO is formed from *NO during a potential sweep in the region from ca. +0.4 to +0.6 V, it will be oxidized or reduced depending on the direction of the scan, at suitable potentials. This implies that the complex behaviour of acidic nitrate solutions on Pt(100) is not a result of nitrate reactivity itself, but of the peculiar behaviour of *NO on this surface facet.

Scheme 1 also explains additional observations for Pt(100) described in the Results section. For example, the complex relationship between the O_1^{100}, R_2^{100} and R_3^{100} shown in Fig. 7 is understood by the higher site occupancy of *NHO compared to *NO on Pt(100). During the O_1^{100} peak, the dehydrogenation of *NHO releases platinum sites which are then free to reduce HNO_3 to *NO in the R_2^{100} peak in the reverse scan. By lowering the potential further, *NO is reduced to *NHO in the R_3^{100} peak. The charge of the O_1^{100} and R_2^{100} peaks depends on the coverage of the previously formed *NHO; a low coverage of *NHO (for example in more concentrated nitrate solutions) will result in a lower current for the *NHO to *NO oxidation (O_1^{100} peak), and thus less free Pt sites for the reduction on HNO_3 to *NO (R_2^{100} peak).

Based on this discussion, we conclude that the complete conversion of nitrate to ammonium on platinum is determined by the reduction of adsorbed NO, which otherwise acts as a poison. For both Pt(111) and Pt(100), *NO is reduced to NH_4^+ in a more negative potential region compared to nitrate reduction to *NO. Under potentiostatic conditions, we anticipate that the complete reduction of nitrate to ammonium is possible only in the potential region where both reactions can take place. From the data shown in Figs. 1 and 2, this condition is fulfilled only by Pt(111), at potentials from ca. +0.25 V to +0.4 V.

4. Conclusions

We summarize below the main findings of our study on the reduction of nitrate in acid:

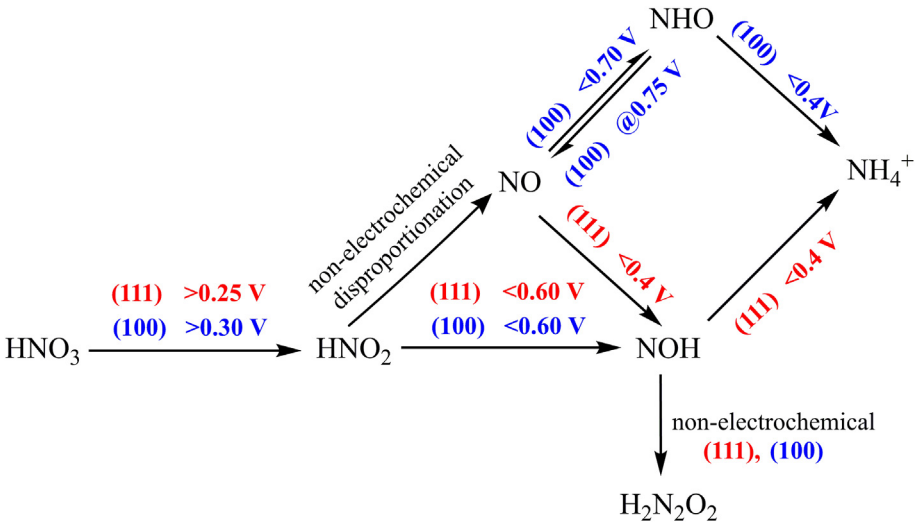

Scheme 1. Proposed scheme for the reduction of HNO_3 to NH_4^+ in acid, depending on the surface structure and the potential. The potentials noted in the scheme are only approximate values.

- On both Pt(111) and Pt(100) HNO_3 is progressively deoxygenated to HNO_2 and *NOH via 2 and 3 electron transfer steps, respectively.
- The formed HNO_2 disproportionates in acid and yields *NO on both surfaces, leading to rapid blocking on Pt(111).
- NO is a key intermediate of nitrate reduction in acid. For the complete reduction of nitrate to ammonium under potentiostatic conditions, *NO reduction to NH_4^+ must be feasible at the same potentials where nitrate reduction to *NO occurs, otherwise the latter acts as a poison.
- The mechanistic structure-sensitivity of *NO reduction renders the mechanism of HNO_3 reduction also structure-sensitive: on Pt(111), *NO is reduced to *NOH at sufficiently low potentials (below +0.4 V for *NO on-top and below +0.25 V for *NO on fcc-hollow sites). On Pt(100), low-coverage *NO is reduced to *NHO already at more positive potentials (i.e. below ca. +0.6 V), but high-coverage *NO requires more negative potentials.
- The formed *NOH will be reduced to NH_4^+ if the potential allows, or will dimerize to $H_2N_2O_2$ on both surfaces.
- The *NHO formed on Pt(100) will be either reduced to NH_4^+ or oxidized back to *NO, depending on the applied potential.

Overall, our study illustrates the complexity of the potential-controlled transformations of nitrogen-containing species on electrified catalytic surfaces. In multi-electron reactions such as nitrate reduction, the complexity stems from the many oxidation states of nitrogen from HNO_3 (+5) to NH_4^+ (−3). In addition, more than one adsorbate or stable product can form at a given oxidation state (for example *NHO, *NOH, N_2O or $H_2N_2O_2$ at an oxidation state of +1) which allows for mechanistic structural sensitivity [5]. This interpretation is general for the nitrogen cycle: nitrate here acts merely as the source of nitrogen-containing adsorbates, which then undergo redox processes depending on the electrode potential and the platinum facet with which it interacts.

Acknowledgements

I.K. acknowledges support by a Marie Curie International Outgoing Fellowship within the seventh European Community Framework Programme (Award IOF-327650). X.C. acknowledges support from the China Scholarship Council (Grant 201506220154). F.C.-V. thanks Spanish MEC for a Ramon y Cajal research contract (RYC-2015-18996) and NWO (Veni Project 722.014.009). The use of supercomputing facilities at SURFsara was sponsored by NWO Physical Sciences, with financial support by NWO. The working electrodes were platinum single-crystals, kindly provided by Prof. Juan Feliù, University of Alicante.

Appendix A. Supplementary data

Supplementary data related to this article can be found at https://doi.org/10.1016/j.electacta.2018.03.126.

References

[1] O.A. Petrii, T.Y. Safonova, J. Electroanal. Chem. 331 (1992) 897–912.
[2] G.E. Dima, G.L. Beltramo, M.T.M. Koper, Electrochim. Acta 50 (2005) 4318–4326.
[3] M.C. Figueiredo, J. Souza-Garcia, V. Climent, J.M. Feliu, Electrochem. Commun. 11 (2009) 1760–1763.
[4] A. Rodes, R. Gómez, J.M. Pérez, J.M. Feliu, A. Aldaz, Electrochim. Acta 41 (1996) 729–745.
[5] I. Katsounaros, M.C. Figueiredo, X. Chen, F. Calle-Vallejo, M.T.M. Koper, ACS Catal. 7 (2017) 4660–4667.
[6] H. Ebert, R. Parsons, G. Ritzoulis, T. VanderNoot, J. Electroanal. Chem. 264 (1989) 181–193.
[7] A. Ahmadi, E. Bracey, R. Wyn Evans, G. Attard, J. Electroanal. Chem. 350 (1993) 297–316.
[8] F.J. Vidal-Iglesias, N. García-Aráez, V. Montiel, J.M. Feliu, A. Aldaz, Electrochem. Commun. 5 (2003) 22–26.
[9] F.J. Vidal-Iglesias, J. Solla-Gullón, V. Montiel, J.M. Feliu, A. Aldaz, J. Phys. Chem. B 109 (2005) 12914–12919.
[10] A.B. Mindler, S.B. Tuwiner, Electrolytic reduction of nitrate from solutions of alkali metal hydroxides, Hydronics Corporation, US Patent 3542657, 1970.
[11] J.D. Genders, D. Hartsough, D.T. Hobbs, J. Appl. Electrochem. 26 (1996) 1–9.
[12] S. Prasad, J. Electrochem. Soc. 142 (1995) 3815–3824.
[13] V. Mani, A.P. Periasamy, S.-M. Chen, Electrochem. Commun. 17 (2012) 75–78.
[14] J. Shen, Y.Y. Birdja, M.T.M. Koper, Langmuir 31 (2015) 8495–8501.
[15] F. Vitse, M. Cooper, G.G. Botte, J. Power Sources 142 (2005) 18–26.
[16] V. Rosca, M. Duca, M.T. de Groot, M.T.M. Koper, Chem. Rev. 109 (2009) 2209–2244.
[17] G.E. Dima, A.C.A. de Vooys, M.T.M. Koper, J. Electroanal. Chem. 554–555 (2003) 15–23.
[18] K. Bouzek, M. Paidar, A. Sadilkova, H. Bergmann, J. Appl. Electrochem. 31 (2001) 1185–1193.
[19] H.-L. Li, J.Q. Chambers, D.T. Hobbs, J. Appl. Electrochem. 18 (1988) 454–458.
[20] D. Reyter, D. Bélanger, L. Roué, Electrochim. Acta 53 (2008) 5977–5984.
[21] G.E. Badea, Electrochim. Acta 54 (2009) 996–1001.
[22] I. Katsounaros, D. Ipsakis, C. Polatides, G. Kyriacou, Electrochim. Acta 52 (2006) 1329–1338.
[23] M.C.P.M. da Cunha, J.P.I. De Souza, F.C. Nart, Langmuir 16 (2000) 771–777.
[24] A.C.A. de Vooys, R.A. van Santen, J.A.R. van Veen, J. Mol. Catal. Chem. 154 (2000) 203–215.
[25] D. Reyter, D. Bélanger, L. Roué, J. Phys. Chem. C 113 (2009) 290–297.
[26] F. Calle-Vallejo, M. Huang, J.B. Henry, M.T.M. Koper, A.S. Bandarenka, Phys. Chem. Chem. Phys. 15 (2013) 3196–3202.
[27] X. Xing, D.A. Scherson, C. Mak, J. Electrochem. Soc. 137 (1990) 2166–2175.
[28] T.Y. Safonova, O.A. Petrii, J. Electroanal. Chem. 448 (1998) 211–216.
[29] G.E. Dima, V. Rosca, M.T.M. Koper, J. Electroanal. Chem. 599 (2007) 167–176.
[30] J. Yang, F. Calle-Vallejo, M. Duca, M.T.M. Koper, ChemCatChem 5 (2013) 1773–1783.
[31] S. Taguchi, J.M. Feliu, Electrochim. Acta 52 (2007) 6023–6033.
[32] S. Taguchi, J.M. Feliu, Electrochim. Acta 53 (2008) 3626–3634.
[33] E.B. Molodkina, I.G. Botryakova, A.I. Danilov, J. Souza-Garcia, J.M. Feliu, Russ. J. Electrochem. 48 (2012) 302–315.
[34] E.B. Molodkina, I.G. Botryakova, A.I. Danilov, J. Souza-Garcia, M.C. Figueiredo, J.M. Feliu, Russ. J. Electrochem. 50 (2014) 370–378.
[35] J. Clavilier, K. El Actii, M. Petit, A. Rodes, M.A. Zamakhchari, J. Electroanal. Chem. 295 (1990) 333–356.
[36] V. Climent, J.M. Feliu, J. Solid State Electrochem. 15 (2011) 1297–1315.
[37] T. Iwasita, F.C. Nart, Prog. Surf. Sci. 55 (1997) 271–340.
[38] J. Yang, Y. Kwon, M. Duca, M.T.M. Koper, Anal. Chem. 85 (2013) 7645–7649.
[39] A. Clayborne, H.-J. Chun, R.B. Rankin, J. Greeley, Angew. Chem. Int. Ed. 54 (2015) 8255–8258.
[40] J.K. Nørskov, J. Rossmeisl, A. Logadottir, L. Lindqvist, J.R. Kitchin, T. Bligaard, H. Jónsson, J. Phys. Chem. B 108 (2004) 17886–17892.
[41] A. Cuesta, M. Escudero, Phys. Chem. Chem. Phys. 10 (2008) 3628–3634.
[42] F.T. Bonner, M.N. Hughes, Comments Mod. Chem. 7 (1988) 215–234.
[43] A. Rodes, V. Climent, J.M. Orts, J.M. Pérez, A. Aldaz, Electrochim. Acta 44 (1998) 1077–1090.